Technology in Cancer Research & Treatment
2017, Vol. 16(6) 900–909

DOI: 10.1177/1533034617708960
journals.sagepub.com/home/tct
SAGE

Assessment of Cryosurgical Device Performance Using a 3D Tissue-Engineered Cancer Model

John M. Baust, PhD[1,2], Anthony Robilotto, MS[1,2], Kristi K. Snyder, PhD[1,2], Kimberly Santucci, BS[1,2], Jennie Stewart, ME[1], Robert Van Buskirk, PhD[1,2,3], and John G. Baust, PhD[2,3]

Abstract

As the clinical use of cryoablation for the treatment of cancer has increased, so too has the need for knowledge on the dynamic environment within the frozen mass created by a cryoprobe. While a number of factors exist, an understanding of the iceball size, critical isotherm distribution/penetration, and the resultant lethal zone created by a cryoprobe are critical for clinical application. To this end, cryoprobe performance is typically characterized based on the iceball size and temperature penetration in phantom gel models. Although informative, these models do not provide information as to the impact of heat input from surrounding tissue nor give any information on the ablative zone created. As such, we evaluated the use of a tissue-engineered tumor model (TEM) to assess cryoprobe performance including iceball size, real-time thermal profile distribution, and resultant ablative zone. Studies were conducted using an Endocare V-probe cryoprobe, with a 10/5/10 double freeze–thaw protocol using prostate and renal cancer TEMs. The data demonstrate the generation of a 33- to 38-cm3 frozen mass with the V-Probe cryoprobe following the double freeze of which ~12.7 and 6.5 cm3 was at or below −20°C and −40°C, respectively. Analysis of ablation zone using fluorescence microscopy 24 hours postthaw demonstrated that the internal ~40% of the frozen mass was completely ablated, whereas in the periphery of the iceball (outer 1 cm region), a gradient of partial to minimal destruction was observed. These findings correlated well with clinical reports on renal and prostate cancer cryoablation. Overall, this study demonstrates that TEMs provide an effective model for a more complete characterization of cryoablation device performance. The data demonstrate that while the overall iceball size generated in the TEM was consistent with published reports from phantom models, the integration of an external heat load, circulation, and cellular components more closely reflect an *in vivo* setting and the impact of penetration of the critical (−20°C and −40°C) isotherms into the tissue. This is important as it is well appreciated in clinical practice that the heat load of a tissue, cryoprobe proximity to vasculature, and so on, can impact outcome. The TEM model provides a means of characterizing the impact on ablative dose delivery allowing for a better understanding of probe performance and potential impact on ablative outcome.

Keywords

thermal ablation, cryosurgery, tissue-engineered model, CryoCare CS system, V-Probe cryoprobe, cell death, prostate cancer, renal cancer

Abbreviations

3D, 3-dimensional; CA, cryoablation; Cal, calcein-AM; PI, propidium iodide.

Received: December 21, 2016; Revised: April 7, 2017; Accepted: April 14, 2017.

Introduction

Cryoablation (CA) of prostate and renal cancers has demonstrated steady growth over the past 10 years. This trend has been reinforced by several long-term follow-up studies showing comparative results between CA and more traditional treatments and the Best Practice guidelines for prostate cryosurgery

[1] CPSI Biotect, Owego, NY, USA
[2] Institute of Biomedical Technology, Binghamton University, Binghamton, NY, USA
[3] Department of Biological Sciences, Binghamton University, Binghamton, NY, USA

Corresponding Author:
John M. Baust, PhD, CPSI Biotect, 2 Court St, Owego, NY 13827, USA.
Email: jmbaust@cpsibiotech.com

issued by the American Urological Association[1-11] Cryoablative therapies represent energy-deprivation strategies dependent on the removal of thermal energy (heat) from the tissues, thereby resulting in controlled, localized freezing. Numerous studies have demonstrated that CA is an effective ablation paradigm engaging several mechanisms including osmotic dehydration, ischemia, intracellular ice formation, and the activation of apoptosis.[12-21] When properly utilized, CA results in a lesion characterized by sharply circumscribed necrosis, persistence of collagen fibers, acellularity, a fibrous stroma, vascular disruption (small vessels only), and the initiation of the wound-healing response that may result in neovascularization.[16,18,19,22,23] A varying cascade of events occurs when cells are cooled. The differential response across the treatment zone is due to the fact that the rate of cooling and final temperature experienced by a cell varies with distance from the cooling source. Nearby cells experience rapid cooling rates, lower temperatures, and intracellular ice. Cells more distant experience extracellular ice, whereas cells even more distant experience only hypothermia. The extent of the "cryolesion" is dependent on a number of factors, including cryogen type (gas, liquid, etc), contact area, cooling rate, temperature, duration of freeze, tissue vascularity, size of the target tumor, and cell sensitivity. The mechanisms underlying the effectiveness of cryosurgery and the optimization of the process have been researched at length. Baust and Gage[12,21-24] reported that while a substantial degree of damage occurs in the -20° to -30°C range, -40°C to -50°C is more effective. It has also been shown that in addition to causing cell rupture and necrosis, freezing activates apoptosis resulting in cell death both rapid and delayed in nature.[22,25-32]

The attractiveness of modern cryoablative therapies is related to numerous factors including a global acceptance of minimally invasive therapies, rapid adoption of intraoperative ultrasound, advances in cryosurgical device technology, and the ability to provide transient, selective protection to adjacent, nontargeted tissues.[5,10,33-38] The key to procedural success is dosimetry in terms of temperature and duration of the freeze–thaw cycle. However, a definitive statement of the "cryoablative dose" has been hampered by the diversity of opinions and practices as they relate to a number of variables, including procedural implementation, cooling "power" (heat extraction capacity of the cryogen), the variability in thermal gradients in frozen tissue, regional blood flow, anatomical variation, cancer's distinct phenotypic responses to a freeze–thaw stress, and the molecular responses of cells of a generically defined "cancer."[22,38-42] Successful CA requires that a targeted volume of tissue be frozen to a lethal target temperature less than -20°C to -40°C (cancer-type dependent) to assure complete lethality throughout the targeted mass.[12,26,40,43] To achieve this goal, a 1-cm positive freeze margin around the targeted tissue volume is typically implemented to assure delivery of a lethal temperature at the tumor margin or risk an increased chance of cancer recurrence. Since the area of the frozen tissue experiencing temperatures above -40°C is confined to the periphery, the volume of this region may equal or exceed the total volume of the targeted ablation zone.[22,24,38] Accordingly, successful application of a cryoablative procedure requires an understanding of the lesion zone and location/distribution of the thermal gradient within the frozen tissue mass between 0°C and -40°C.

In order to determine the impact of various cryosurgical devices and protocols, we have developed a novel 3-dimensional (3D) tissue-engineered model tissue–engineered tumor model (TEM) to assess the destructive effectiveness of cryoablative devices.[32,44] TEM allows for the real-time assessment of thermal profiles generated by a cryoprobe, size of the iceball created, as well as determination of the lethal zone created (live and dead zones within the tissue) in situ via fluorescence imaging at various time points following freezing.[41,45] Furthermore, the model allows for determination of how far within the overall frozen mass various isotherms are when utilized in a heat-loaded setting. The development and use of tissue-engineered models in preclinical testing provide a useful tool for the assessment of devices and probes to benchmark performance. This system also allows one to compare the impact of modifications/improvements to a device or procedures as well as between devices. This is especially beneficial in light of the ever-increasing demand by regulatory bodies to reduce/eliminate animal testing.[46,47] Although not a complete replacement for preclinical animal studies, these models are now providing an effective bridge between phantom nonliving models (ultrasound and/or agarose gels, water baths, etc) and animal studies. The use of TEMs provides for a reliable, reproducible, and cost-effective testing platform during the initial product and protocol development and optimization stages.[41]

Based on the growing use of CA to treat numerous cancers and the importance of achieving a desired critical temperature (ie, -20°C or -40°C) coupled with limited technical ability to monitor temperatures throughout a tumor during a procedure in real time, we used 2 TEMs (prostate and renal) to characterize the performance of a commercial CA device and associated cryoprobe. This was conducted in an effort to evaluate the TEM, characterize device performance, and correlate the performance with the delivery of an ablative insult. The data presented herein demonstrate that the TEMs served as an effective model for evaluating cryoprobe performance. To this end, the TEM allowed for the generation of an overall iceball consistent with that reported in other models while enabling characterization of the thermal profile generated within the frozen mass in real time as well as the assessment of the ablative zone generated within the frozen mass.

Methods

Cell and 3D Cultures

The human prostate (PC-3) and renal (786-O) cancer cell lines were obtained from the ATCC (Rockville, Maryland). Cultures were maintained at 37°C, 5% CO_2:95% air in RPMI-1640 culture medium (Caisson Laboratories Inc, North Logan, Utah) fortified with 10% FBS (Atlanta Biologics Inc, Atlanta,

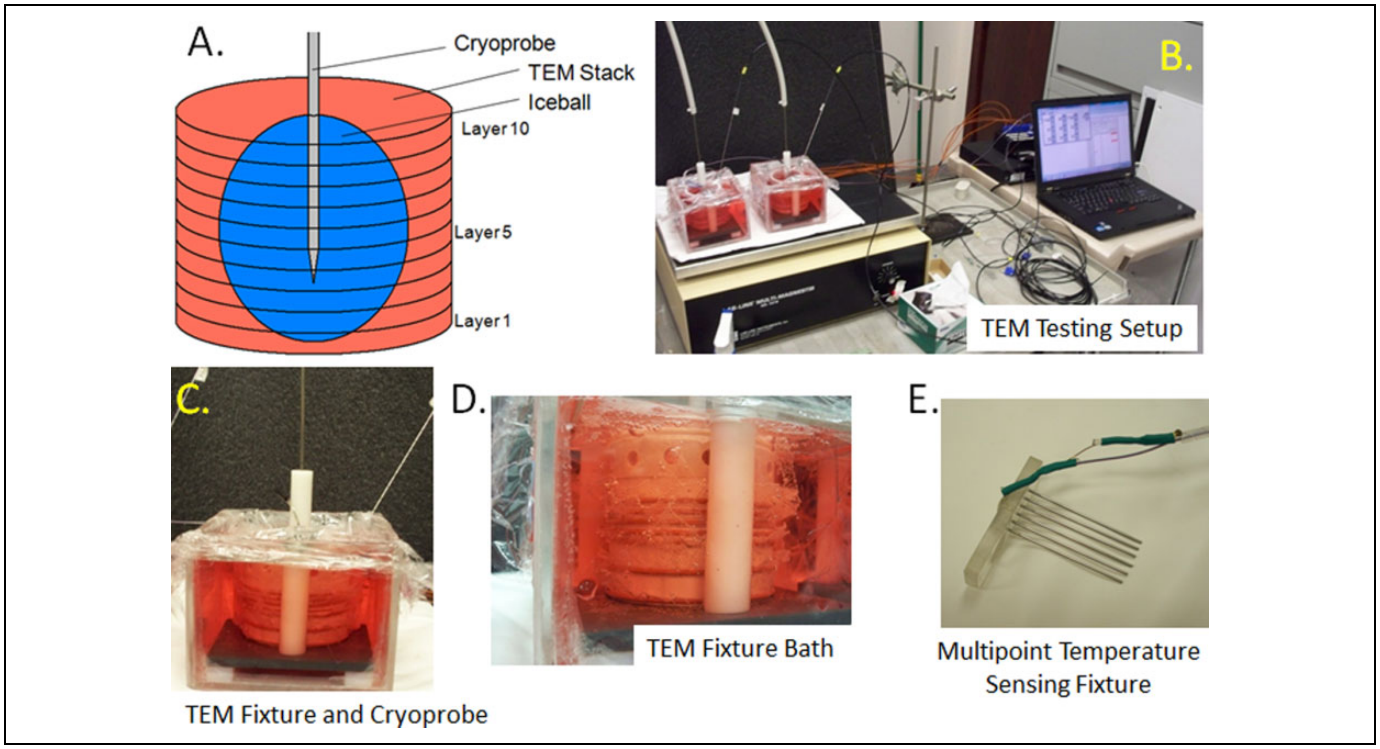

Figure 1. Images of TEM freeze apparatus setup. TEMs were assembled into 3D stacks and placed into a bath of warm media on a warming pad and a stir table to facilitate circulation of the media bath during the freezing process. Cryoprobe was then placed into the center of the TEM and positioned 9 mm from the bottom of the TEM stack. Temperatures of the bath and within the TEM gels were monitored throughout the freeze protocol. A, Schematic of a multilayered TEM stack with cryoprobe inserted and iceball; (B) image of a full testing freeze setup including TEM fixtures, cryoprobe, heat source, stir table, TempScan, and PC monitoring station; (C) close up of an individual TEM apparatus; (D) profile photo of the TEM stack configuration during a freeze procedure; and (E) illustration of the thermocouple array inserted in the TEMs to monitor temperature distribution radiating from the center point of the cryoprobe ablation segment. 3D indicates 3-dimensional.

Georgia) and 1% penicillin/streptomycin (Corning, Inc, Corning, New York). Cells were cultured in 75 cm^2 t-flasks with media replenishment every 3 days.

For generation of the tissue-engineered models (TEM), rat tail type I collagen solution (BD Bioscience, Bedford, Massachusetts) was used to form 0.2% wt/vol gel matrices as per standard protocol. Cells, prostate 0.85 to 1.2 $\times 10^6$ cells/mL and renal 0.65 to 0.8 $\times$ 10^6 cells/mL, were suspended in the collagen solution prior to solidification in 3 mm $\times$ 60 mm TEM ring fixtures as per Robilotto et al and Baust et al.[32,44,48] The TEM cell containing matrices were cultured for 24 hours prior to utilization. All experiments were performed between cell passages 5 and 20.

Freezing Protocol

Prior to freezing, individual cell-seeded TEMs were assembled into the 3D stack configuration (60 mm $\times$ 60 mm) following SOP. The TEM stack was then submerged into a warm circulating bath of culture media followed by placement onto a heat pad and stir table, and a cryoprobe and thermocouple array were then inserted to monitor temperatures (Figure 1). Samples were held until TEM and bath temperatures equilibrated at 32°C ($\pm$2°C); TEM samples were frozen using the CryoCare CS cryosystem (EndoCare, Inc, Austin, Texas) using a 2.4 mm V-Probe cryoprobe (EndoCare, Inc.) set to either 3-cm (prostate) or 4-cm (renal) freeze zone length. TEM models were frozen using a 10/5/10 (in minutes) freeze/thaw/freeze protocol. Temperature of the bath and within the TEM were monitored throughout the freezing process at fixed distances of 7.5, 10.5, 13, 16, and 19 mm extending radially from the surface of the cryoprobe at the center point of the freeze zone (ie, 1.5 cm for prostate and 2 cm for renal studies) using an type-T thermocouple array and recorded with a Omega TempScan at 10-second intervals throughout the entire freeze cycle. At the completion of the freeze cycle, TEMs were allowed to passively thaw in the warm circulating bath for 30 minutes prior to disassembly at which time the individual TEM layers were returned to culture for recovery and assessment.

TEM Assessment

Following thawing and disassembly, individual TEM layers were measured via calipers to determine the diameter of the iceball created following the first and second freezes of the freeze–thaw cycle (Figure 2). Iceball radii were also measured at cardinal locations around the probe surface to determine symmetry of the freeze zone created. Individual layers were

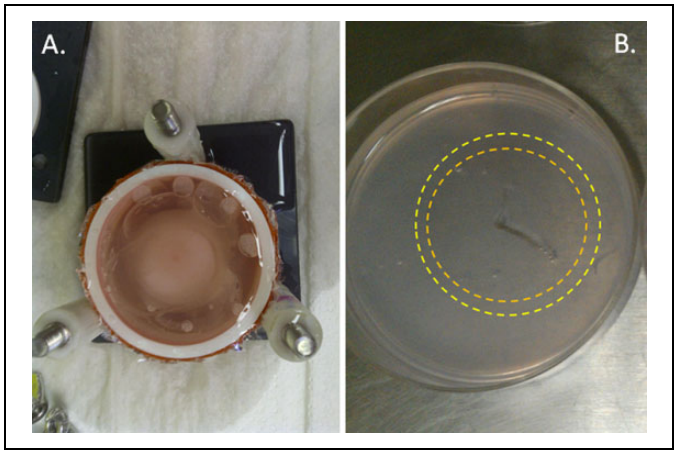

Figure 2. Image of a TEM stack and layer following freezing. TEM stacks were frozen in the TEM assembly apparatus. Following freezing, TEM stacks were disassembled into individual layers for assessment of iceball diameter as well as cell destruction using fluorescent microscopy. A, Top view of a TEM stack following freezing prior to stack disassembly and (B) image of an individual TEM layer in culture following disassembly. During analysis, identification of the outer edge of the first (orange ring) and second freeze (yellow ring) iceball edge (transition from frozen to nonfrozen tissue which equates to $\sim -2^{\circ}C$, nominally) is visible within the gel, thereby allowing for direct measurement of iceball diameter following each freeze event within the protocol.

then cut into half (bisection of the probe center) yielding 2 replicate samples from each layer for analysis. One half of the layer sample was then placed into culture to assess 24 hours postfreezing recovery, whereas the other half was assessed for immediate (1 hour) postfreeze viability. In situ sample viability assessment was performed using the fluorescent probes calcein-AM and propidium iodide (Cal/PI; Invitrogen, Carlsbad, California). Briefly, culture medium was decanted from the TEM samples, and 2 mL of the working Cal/PI solution (10 µL Cal + 8 µL PI + 2 mL phosphate-buffered saline) was added directly to each sample. Samples were incubated in the dark at 37°C for 60 (±1) minutes. Fluorescent staining was visualized using a Zeiss Axiovert 200 fluorescent microscope under a 10× magnification with the AxioVision 4 software (Carl Zeiss, Germany). Panoramic digital images were recorded starting at the iceball center (probe surface) and extended across the freeze region into the nonfrozen periphery. Following acquisition, a 5000 µm (5 mm) scale bar and reference mark at a radius of 15 mm (represent a 3 cm diameter) were autoimprinted onto each of the images using the AxioVision software to enable direct image comparison.

Data Analysis

For iceball and thermal profile assessment, a minimum of 7 repeats per probe setting were conducted. For ablation zone imaging studies, a minimum of 3 TEM repeats per cancer type (prostate and renal) were conducted. Following experimentation, data were combined and averaged (±standard deviation) to determine mean iceball size, temperature location, and ablation zone produced. Iceball, thermal zone, and ablation volumes were calculated based on freeze zone center point TEM layer measurements using an ellipsoid model to enable volumetric analysis of system performance.

Table 1. Average Measurements of the Iceball Created by a V-Probe in the TEM Following a 10/5/10 Freeze.

	Average Iceball Diameter, cm (SD)		Iceball Volume
	First Freeze	Second Freeze	Second Freeze, cm^3
pTEM	3.65 (±0.09)	4.27 (±0.13)	33.40
rTEM	3.83 (±0.12)	4.63 (±0.21)	38.76

Abbreviation: SD, standard deviation.

Freeze zone size. Following the freeze/thaw episode, iceball diameter and radii were measured using digital calipers at the center point of the cryoprobe freeze zone.

Ablation zone. Fluorescent imaging of the TEM at the center point of the cryoprobe, images were measured using the AxioVision software to determine the size of the zone of ablation (PI-positive/Cal-negative [red] region).

Thermal profiles. Real-time recordings of the thermal profiles collected using the Omega TempScan system were converted to graphical format using Microsoft Excel and analyzed to determine isotherm spread during the first and second freeze intervals.

Results

Cancer Cell Ablation Comparison Studies

A series of studies were conducted utilizing tissue-engineered prostate (pTEM) and renal (rTEM). For the pTEM, experiments were performed using a 2.4-mm V-Probe cryoprobe set at a 3-cm freeze zone length (2.4 mm × 3 cm freeze zone) for the analysis of freezing and prostate cancer cell destruction. For the rTEM, experiments were performed using a V-Probe cryoprobe set at a 4-cm freeze zone length (2.4 mm × 4 cm freeze zone). The 3-cm and 4-cm freeze zone lengths were selected as per manufacture recommendations for prostate and renal tumor application.

Iceball analysis and comparison. For assessment of overall iceball size following the freeze interval, pTEM (prostate cancer) samples were frozen using the 10/5/10 protocol, allowed to thaw, and then disassembled into individual layers. The layers were then measured to determine the size (diameter) of the frozen mass following the first and second freeze episode. This assessment was possible following thawing as each ice front left a distinct visible ring where the edge of the iceball was (Figure 2). These rings represented the transition from frozen to nonfrozen TEM tissue and correlate with a temperature of $\sim -2^{\circ}C$. Assessment of iceball diameter following freezing of the pTEM using the 2.4 mm × 3 cm V-Probe cryoprobe revealed an average diameter of 3.65 (±0.09) cm following the first freeze and 4.27 (±0.13) cm following the second freeze (Table 1).

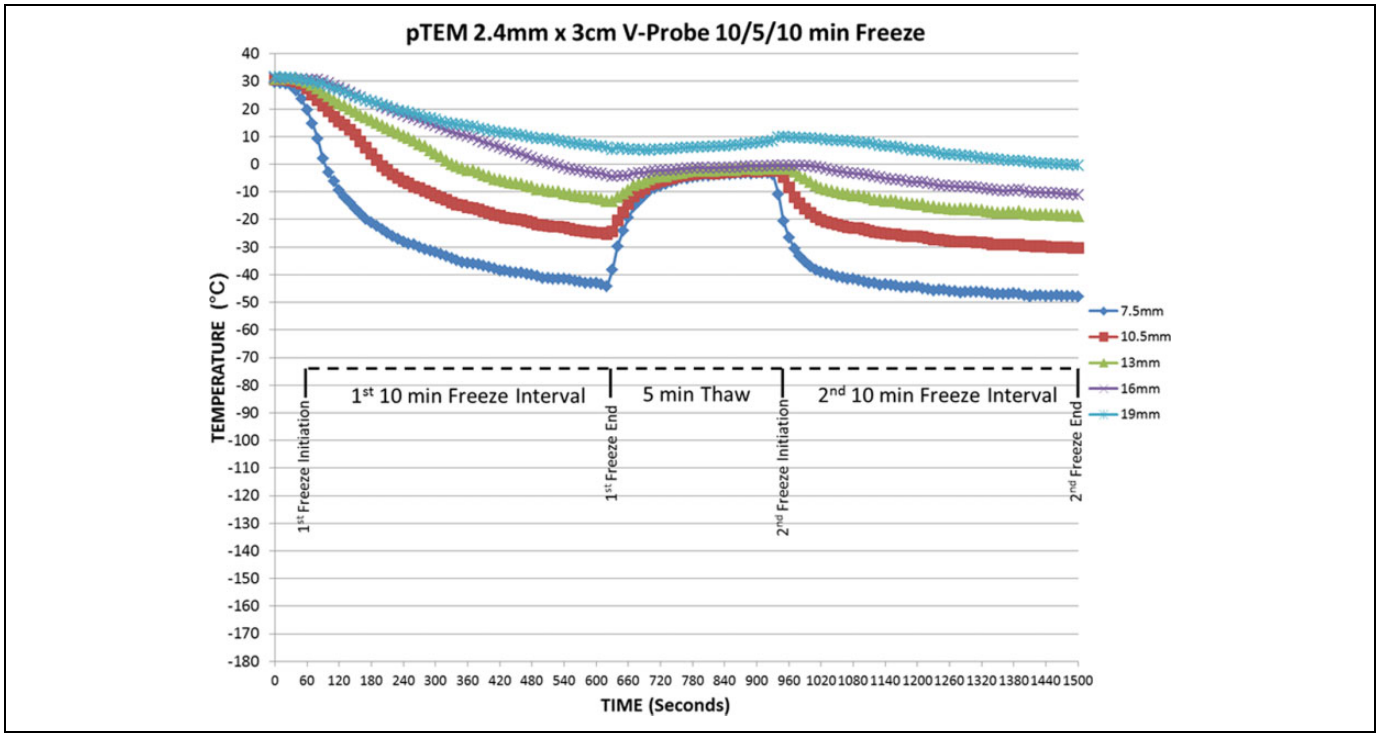

Figure 3. Real-time monitoring of pTEM (prostate cancer) temperatures at the center of the freeze length during a 10/5/10 freezing protocol. Temperatures of the midpoint TEM layer were monitored at fixed points radiating from the cryoprobe surface in real time at 10-second intervals during a 10/5/10 freeze/thaw/freeze procedure. Temperatures were found to drop radially near the probe surface and were more gradual the further from the probe surface. Thermal profile assessment revealed a final penetration of the −20°C and −40°C isotherms to reach diameter of 2.6 and 1.8 cm, respectively. Analysis of the thermal profiles revealed that on average 39% and 19% of the frozen mass was encompassed within the −20°C and −40°C isotherms, respectively.

Volumetric analysis of the iceball formed by the V-Probe cryoprobe revealed a 33.4-cm^3 frozen mass following the second freeze.

For assessment of overall iceball size created using the 2.4 mm V-Probe cryoprobe with a 4-cm freeze zone length (2.4 mm × 4 cm), rTEM (renal cancer) samples were frozen under the 10/5/10 protocol. As with pTEM samples, the TEM layer at the center of the freeze length was measured to determine the size (diameter) of the frozen mass following the first and second freeze. Assessment of iceball diameter following freezing of the rTEM revealed the formation of an iceball with an average diameter of 3.83 (±0.12) cm following the first freeze and 4.63 (±0.21) cm following the second freeze (Table 1). Volumetric analysis of the iceball formed by the V-Probe cryoprobe revealed 38.8 cm^3 iceball on average following the second freeze. The formation of a larger iceball created by the V-Probe cryoprobe in the rTEM compared to the pTEM was expected given the 23% increase in freeze zone surface area of the V-Probe cryoprobe set at 4 cm compared to the 3-cm freeze zone length, which translated to a ∼17% increase in the overall volume of the iceball.

pTEM isotherm analysis and comparison. Although iceball size is often utilized as a comparative metric for the performance of cryosurgical devices, the size of the iceball generated does not reflect isotherm distribution within the frozen mass. Given this, assessment of isothermal distribution within the frozen mass was monitored in real time during freezing. Assessment of the thermal profile was conducted at 5 fixed positions extending from the probe surface at the center of the probe freeze zone (Figure 3). Isotherm assessment studies conducted using the 2.4 mm × 3 cm V-Probe cryoprobe following the 10/5/10 protocol revealed an isothermal profile characterized by the −20°C isotherm at a diameter of 2.28 (±0.17) cm and 2.63 (±0.21) cm following the first and second 10-minute freeze, respectively (Table 2). Examination of the −40°C isotherm revealed a 1.6 (±0.1)-cm and 1.87 (±0.13)-cm diameter following the first and second freeze, respectively. Volumetrically, this correlated with 12.67 and 6.41 cm^3 of the 33.4 cm^3 frozen mass being at or below −20° and −40°C, respectively. Comparing the penetration of the lethal isotherm to that of the overall frozen mass created by the V-Probe cryoprobe, it was found that 37.9% and 19.1% of the total volume of the frozen TEM was ≤−20°C and −40°C, respectively.

As with the prostate cancer pTEM studies, assessment of the isothermal profile following the initial 10 minutes of freezing of the rTEM using the 2.4 cm × 4 cm V-Probe cryoprobe revealed a lethal −20°C isotherm at a diameter of 2.37 (±0.19) cm and the −40°C isotherm at a diameter of 1.8 (±0.12 cm; Table 2) cm. After completion of the second 10-minute freeze, the −20°C and −40°C isotherm diameters were found to extend to 2.6 (±0.23) cm and 1.8 (±0.12) cm,

Table 2. Analysis of Critical Isotherm Penetration, Volume, and Percentage of Frozen Mass Contained Within the Isotherm Following a 10/5/10 Freeze With the V-Probe in the TEM.

	Average Lethal Isotherm Diameter, cm (SD)				Volume, cm^3		% of Iceball	
	First Freeze		Second Freeze		Second Freeze		Second Freeze	
	−20°C	−40°C	−20°C	−40°C	−20°C	−40°C	−20°C	−40°C
pTEM	2.28 (±0.17)	1.60 (±0.1)	2.63 (±0.21)	1.87 (±0.13)	12.67	6.41	37.90	19.20
rTEM	2.37 (±0.19)	1.80 (±0.12)	2.60 (±0.23)	1.80 (±0.12)	12.88	6.27	31.90	15.30

Abbreviation: SD, standard deviation.

respectively. Volume equaled 12.38 and 6.27 cm^3 out of the total 38.76 cm^3 frozen mass being at or below −20° and −40°C, respectively. In relation to the overall iceball volume following the 10/5/10 protocol, 31.9% of the iceball was at −20°C or below and 16.1% was at or below −40°C.

Fluorescent microscopy imaging and comparison. With the thermal characterization of the frozen mass created within the TEM for the 2.4-mm V-Probe cryoprobe, image analysis utilizing fluorescent microscopy was conducted to evaluate the overall ablative impact. To evaluate the level of cellular destruction, examination of the TEM layer at the center of the probe freeze zone was conducted following completion of a 10/5/10 double freeze protocol. In addition to analysis at the center of the freeze zone, vertical profiling of the lethal zone was also conducted. Fluorescent imaging to visualize living (green) versus dead (red) cancer cells was conducted at 1 and 24 hours postfreeze. The 1- and 24-hour time points were selected to allow for the assessment of immediate cell death as well as for identification of any delayed cell responses (death or recovery) within the TEM, such as in the periphery where sublethal freezing temperatures are achieved (ie, warmer than −30°C for prostate cancer). It is within this partially ablated region where both *in vitro* and *in vivo* studies have concluded that incomplete cancer cell destruction can lead to recovery postfreeze and has been identified as a potential source for cancer recurrence.

Analysis of prostate cancer cell destruction following freezing with the 2.4 mm × 3 cm V-Probe cryoprobe revealed near complete cell destruction extending to 1.34 (±0.1) cm from the probe surface yielding a 2.67 (±0.21)-cm diameter lethal zone around the cryoprobe at the center of the freeze zone (Figure 4). Correlating the zone of destruction with the isotherm profile data revealed a transition from cell destruction to survival occurring around the −20°C isotherm (Figure 4B). This resulted in a 0.4 (±0.1)-cm rim of incomplete cell destruction within the perimeter of the iceball observed 1 hour postfreeze. Interestingly, when follow-up analysis was conducted at 24 hours postfreeze, a substantial level of cell recovery in the periphery was noted (Figure 4C). The recovery was not attributed to cell regrowth given the short interval (24 hours) but was likely a result of "injured cells," which experienced damaging sublethal temperatures recovering.

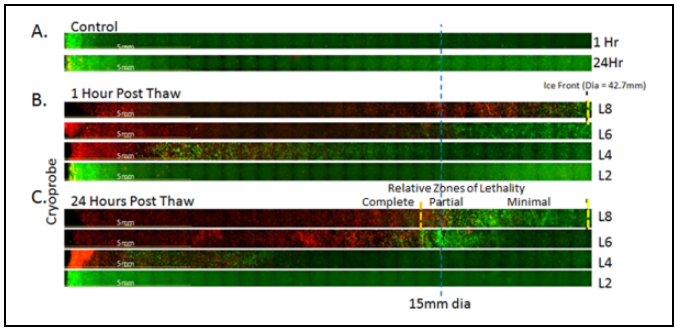

Figure 4. Representative panoramic fluorescent images of pTEM (prostate cancer) layers at 1 and 24 hours following freezing. TEMs were frozen under a 10/5/10 minute freeze/thaw/freeze protocol using a 2.4-mm V-Probe set with a 3-cm freeze length. Following freezing, individual TEM layers were dissembled and placed into culture for assessment in comparison with controls (A). Following 1 (B) and 24 (C) hours of recovery replicate, TEM layers were probed with calcein-AM (green) and propidium iodide (red) and visualized using fluorescence microscopy to determine the extent of cell death. Cryoprobe was located at the left of the images. The blue line marks a 1.5 cm radial distance from the probe. The yellow dashed line indicated the edge of the iceball following the second freeze. The orange dashed line represents the approximate location of the −30°C isotherm indicating the transition from partial to complete cell lethality. Layer 2 (L2) was located just below the cryoprobe tip, L4 at the probe tip (0.1 cm), L6 1/4 up (0.75 cm), and L8 at the midpoint (1.5 cm) of the cryoprobe freeze zone. Analysis of cell death at 24 hours postfreeze revealed average lethal zone equivalent to 39% of the frozen mass.

The 24-hour time point has been reported to more accurately reflect cell death caused by freezing compared to 1 hour postfreeze. When correlating the observed lethal zone at 24 hours with the overall iceball, a 0.8 (±0.2)-cm wide rim of incomplete destruction within the periphery of the iceball was produced. This equated to a temperature of ∼−30°C based on the thermal profile data. Freeze zone profile analysis utilizing pTEM layers ranging from the tip to the center of the cryoprobe freeze zone revealed the formation of a characteristic oval-like ablation zone tapering toward the top of the cryoprobe. The transition of the iceball between the vertical layers was found to be smooth yielding the oval-like ablation zone. As with the freeze zone center layer, comparison of 1-hour samples to 24-hour samples revealed a substantial level of cancer cell recovery within the periphery of the iceball. Calculations of ablative volume

Table 3. Comparison of Average Iceball Size and Zone of Cancer Cell Ablation Within the TEM Created by the V-Probe Following a 10/5/10 Minute Freeze.

	Iceball Size		Zone of Ablation		
	Diameter, cm (SD)	Volume, cm^3	Diameter, cm (SD)	Volume, cm^3	% Iceball
pTEM	4.27 (±0.3)	33.40	2.67 (±0.21)	13.06	39.11
rTEM	4.63 (±0.4)	38.76	2.80 (±0.28)	14.36	37.05

Abbreviation: SD, standard deviation.

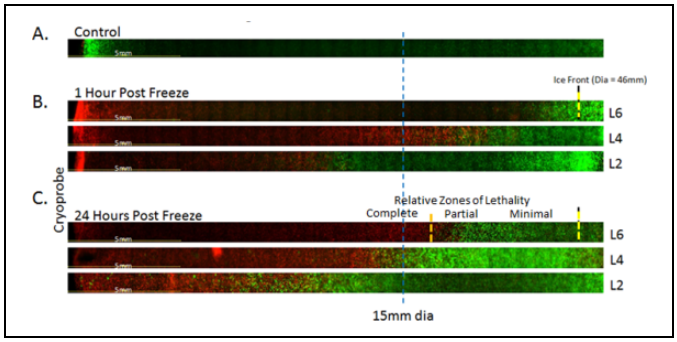

Figure 5. Representative panoramic fluorescent images of rTEM (renal cancer) layers at 1 and 24 hours following freezing. TEMs were frozen under a 10/5/10 minute freeze/thaw/freeze protocol using a 2.4-mm V-Probe set with a 4-cm freeze length. Following freezing, individual TEM layers were dissembled and placed into culture for assessment in comparison with controls (A). Following 1 (B) and 24 (C) hours of recovery replicate TEM layers were probed with calcein-AM (green) and propidium iodide (red) and visualized using fluorescence microscopy to determine the extent of cell death. Cryoprobe was located at the left of the images. The blue line marks a 1.5-cm radial distance from the probe. The yellow dashed line indicated the edge of the iceball following the second freeze. The orange dashed line represents the approximate location of the −20°C isotherm, indicating the transition from partial to complete cell lethality. Layer 2 (L2) was at 0.5 cm up from the cryoprobe tip, L6 1/4 up (1.25 cm), and L6 at the midpoint (2 cm) of the cryoprobe freeze zone. Analysis of cell death at 24 hours postfreeze revealed an average lethal zone equivalent to 37% of the frozen mass.

based on fluorescent imaging revealed an ablative volume of 13.06 cm^3, which equated to ∼39% of the frozen mass at 24 hours postfreeze (Table 3).

Image analysis utilizing fluorescent microscopy was then conducted using the renal cancer rTEM 3D model. Given the published increased sensitivity of renal cancer (compared to prostate cancer) to low-temperature exposure,[26] studies were conducted to determine what effect the freeze procedure had on renal cancer cell destruction at the center of the probe freeze zone (2 cm level) following completion of a 10/5/10 protocol (Figure 5). In addition to analysis at the center of the freeze zone, vertical profiling of the lethal zone was also conducted at 1 and 24 hours postfreeze.

Analysis of renal cancer cell destruction following freezing revealed near complete cell death to an average distance of 1.9 (±0.15) cm from the probe surface, yielding a ∼3.8 (±0.3)-cm diameter lethal zone around the cryoprobe at the center of the freeze zone at 1 hour postfreeze (Figure 5B). Correlating the zone of destruction with the isotherm profile data revealed the transition from cancer cell destruction to survival was around the −15°C isotherm at 1 hour postfreeze. As a result, a 0.4 (±0.15)-cm wide rim of incomplete cell destruction was found to remain around the perimeter of the iceball. Interestingly, as with the pTEM samples, when follow-up analysis was conducted at 24 hours postfreeze, a substantial level of cell recovery was noted in the periphery (Figure 5C). Correlating the observed 24-hour lethal zone to the overall iceball revealed a 0.9(±0.2)-cm deep rim of incomplete destruction within the periphery of the iceball, revealing the actual lethal isotherm to be ∼−20°C. This was consistent with previous *in vitro* reports.[26] Freeze zone profile analysis of rTEM layers ranging from the tip to the center of the cryoprobe freeze zone again revealed the formation of an oval-like ablation zone. Further, similar to the freeze zone from the center layer of the rTEM, comparison of 1-hour samples to 24-hour samples through the vertical stack revealed a substantial level of cancer cell recovery within each layer in the periphery of the iceball. Analysis of the ablative zone in the rTEM via fluorescence imaging revealed an ablative zone of ∼14.36 cm^3 within the 38.78 cm^3 frozen mass. Therefore, ∼38% of the iceball was lethal at 24 hours postfreeze following the double freeze 10/5/10 protocol (Table 3).

Discussion

This study examined the use of a 3D tissue-engineered tumor model (TEM) of prostate and renal cancer for the evaluation of the performance of a cryosurgical device. The findings demonstrate that the TEMs were provided for an effective medium for the assessment of several performance indicators including iceball size, thermal profiling (isotherm distribution), and the resultant lethal zone within the frozen mass following thawing. With a variety of parameters being investigated in this study, including differing probe freeze zone length (3 and 4 cm) and cancer type (prostate and renal TEMs), extensive characterization and comparative data were generated. Although each of the parameters had an impact on an individual group's outcome, several fundamental comparatives emerged from the data. When looking at iceball diameter, the freeze protocol of 10/5/10 in conjunction with the V-Probe cryoprobe with a 4-cm length consistently yielded a larger iceball than when the 3-cm freeze zone length. This was an anticipated outcome given the ∼23% larger surface area (31.6 vs 37.2 cm^2). Although the iceball diameter was found to be larger, analysis of the critical

isotherms within the frozen mass revealed similar penetration of the −20°C and −40°C isotherms into the TEM following the 10/5/10 protocol (Table 2), meaning that the additional ~5.5 cm^3 of ice generated in the rTEM represented nonlethal ice. Analysis of the level of cell destruction (distance from the cryoprobe) in the pTEM and rTEM following freezing using fluorescent imaging revealed that, similar to the isotherm data, the volume of cell death observed in the samples was similar to the transition zone from living to dead cancer cells being an average of 1.34 cm from the cryoprobe, yielding a 2.67-cm diameter lethal zone in the prostate cancer pTEM samples and a diameter of 2.8 cm in the rTEM. The increased size of the ablative zone in the rTEM compared to the pTEM was anticipated and consistent with the literature where it has been established that renal cancer has a greater thermal sensitivity than prostate cancer to mild freeze insults. Interestingly, despite the apparent larger lethal zone in the rTEM samples, when normalized to the overall iceball size, the destructive volume of the respective iceballs was similar, approaching ~40% of the total volume in both prostate and renal TEMs (Table 3).

When comparing our findings with the reported V-Probe cryoprobe performance data[49] on iceball size generated following a 10-minute freeze, the iceballs generated within the TEMs correlated closely for both 3- and 4-cm freeze lengths. Specifically, published reports using a gelatin phantom model indicate an iceball diameter of 3.9 (±0.5) cm and 3.8 (±0.5) cm for the 4- and 3-cm freeze lengths and in the TEM iceball diameters of 3.83 and 3.65 cm were obtained.[49] Interestingly, the −20°C and −40°C isotherms were found to not penetrate as far within the TEMs than reported in the gelatin phantom. For instance, in the pTEM with the 2.4 mm × 3 cm freeze zone, the −20°C was found to have a diameter of 2.28 (±0.17) cm following a 10-minute freeze versus the reported 2.54 (±0.5) cm diameter in the gelatin phantom. Similarly, the −40°C isotherm was found to have a diameter of 1.6 (±0.1) cm in the TEM versus 1.8 (±0.5) cm in the gelatin phantom. Similar results were also seen with the 2.4 mm × 4 cm freeze zone in the rTEM setting. The smaller diameter of the −20°C and −40°C isotherms in the TEM compared to the gelatin phantom was expected as the TEM integrates in active heat input and circulation components into the model in an effort to deliver a test environment which more closely reflects an *in vivo* setting where circulation and heat from surrounding tissue continuously impact the iceball. This affects both overall iceball size and to a greater extent the isothermal profile within the frozen mass *in vivo*. The incorporation of active heat input coupled with circulation during the freeze/thaw procedure provides for a more stringent testing setup, thereby creating a more *in vivo*-like testing environment. Although more reflective from the heat input perspective, the TEM has limitations, however, given that it does not incorporate/account for any immunological, wound healing or long-term ischemic injury damage which occurs *in vivo* following freezing. To this end, based on its nature and tissue culture environment, the TEM represents a near ideal environment for sample recovery as it provides for optimal oxygen and nutrient delivery throughout the sample. As such, when translating/comparing these results to *in vivo* scenarios, as with data from all *ex vivo* and phantom models, caution should be taken.

Another interesting observation was the propensity for cell recovery within the periphery of the frozen mass. For instance, initial analysis of the pTEM samples at 1 hour postfreeze suggested ~50% lethality within the frozen mass; however, analysis at 24 hours revealed 39% lethality (Figure 4). Similarly with rTEM samples, 1 hour analysis suggested ~60% iceball lethality, whereas at 24 hours postfreeze, the actual lethality was found to be 37% (Figure 5). The observed recovery within the periphery of the iceball is hypothesized to be a result of the repair and recovery of partially damaged (injured) cancer cells exposed to mild freezing temperatures (>−20° to −30°C). The observed "increased cell lethality" at 1 hour compared to 24 hours postfreeze may also be a result of increased permeability in the cellular membranes within the periphery resulting in increased uptake of propidium iodide during the early stages of recovery resulting in surviving cells appealing dead early on thereby resulting in a false positive. Although the temperature range varies, this survival and recovery phenomena have been documented in numerous cancer types, including renal and prostate, and have been hypothesized to be a potential source of disease recurrence *in vivo*.[16,38,43] To this end, in this study, a ~0.8-cm rim of surviving cells was found within the periphery of the iceball in the pTEM and a 0.9-cm rim in the rTEMs. The transition of completely too partially dead cells correlated with a temperature of ~−30°C in the pTEM and ~−20°C in the rTEM. These findings correlate well with previous reports and clinical observations where a ~1-cm positive freeze margin is used to assure delivery of an ablative dose (−30°C to −40°C in prostate cancer and −20°C to −30°C in renal cancer) to the tumor margin to assure complete cancer destruction.[1,12,17,19,35,36,43] As such, the findings of a 0.8- and 0.9-cm transition zone from live to dead cells at the outer edge of the iceball in this study were similar to clinical observations. It is a result of this phenomenon that the standard practice of incorporating a 1-cm positive freeze margin to assure attainment of a critical temperature within a target tissue has been incorporated clinically.[1,22,35]

In conclusion, the data from this study suggest that TEMs provide for an effective model for the characterization of CA device performance including iceball size, thermal profiling (isotherm distribution), as well as the resultant lethal zone within the frozen mass following thawing. Using this model, it was shown that the V-Probe cryoprobe delivered an ablative dose (<−20°C) ~1 cm within the edge of the iceball. This correlated with the creation of an overall lethal zone of ~40% of the total volume within the frozen mass in both the prostate cancer and renal cancer TEMs under physiological relevant a heat load challenge. The data demonstrated that though the overall iceball size generated in the TEM was consistent with published reports from phantom models, the addition of the heat load and circulation to more closely reflect an *in vivo* setting impacted the penetration of the critical (−20°C and −40°C) isotherms into the tissue. This is an important

observation as it is well appreciated in clinical practice that the heat load of a tissue, cryoprobe proximity to vasculature, and so on can impact the outcome. The TEM provides a means of characterizing this impact on ablative dose delivery, resulting in a better understanding of probe performance and impact on outcome. This in turn may provide an avenue for improved device development, procedure application, and ultimately improved clinical outcome.

Acknowledgments

The authors wish to express their appreciation to Mr. Alind Sahay, MS, MBA for his diligent efforts in the execution of these studies.

CRYOCARE CS, ENDOCARE and V-PROBE are trademarks of Endocare, Inc., registered in the United States with the U.S. Patent and Trademark Office and in other countries.

Declaration of Conflicting Interests

The author(s) declared no potential conflicts of interest with respect to the research, authorship, and/or publication of this article.

Funding

The author(s) disclosed receipt of the following financial support for the research, authorship, and/or publication of this article: This study was supported in part by funding from EndoCare, Inc.

References

1. Babaian RJ, Donnelly B, Bahn D, et al. Best practice statement on cryosurgery for the treatment of localized prostate cancer. *J Urol*. 2008;180(5):1993-2004.
2. Cohen JK, Miller RJ Jr, Ahmed S, Lotz MJ, Baust J. Ten-year biochemical disease control for patients with prostate cancer treated with cryosurgery as primary therapy. *Urology*. 2008; 71(3):515-518.
3. Long JP, Bahn D, Lee F, Shinohara K, Chinn DO, Macaluso JN Jr. Five-year retrospective, multi-institutional pooled analysis of cancer-related outcomes after cryosurgical ablation of the prostate. *Urology*. 2001;57(3):518-523.
4. Bahn DK, Lee F, Badalament R, Kumar A, Greski J, Chernick M. Targeted cryoablation of the prostate: 7-year outcomes in the primary treatment of prostate cancer. *Urology*. 2002;60(2 suppl 1):3-11.
5. Bahn D, de Castro Abreu AL, Gill IS, et al. Focal cryotherapy for clinically unilateral, low-intermediate risk prostate cancer in 73 men with a median follow-up of 3.7 years. *Eur Urol*. 2012;62(1): 55-63.
6. Spiess PE, Given RW, Jones JS. Achieving the 'bifecta' using salvage cryotherapy for locally recurrent prostate cancer: analysis of the Cryo On-Line Data (COLD) registry data. *BJU Int*. 2012; 110(2):217-220.
7. Spiess PE, Levy DA, Pisters LL, Mouraviev V, Jones JS. Outcomes of salvage prostate cryotherapy stratified by pre-treatment PSA: update from the COLD registry. *World J Urol*. 2013;31(6):1321-1325.
8. Williams AK, Martínez CH, Lu C, Ng CK, Pautler SE, Chin JL. Disease-free survival following salvage cryotherapy for biopsy-proven radio-recurrent prostate cancer. *Eur Urol*. 2011;60(3): 405-410.
9. Wenske S, Quarrier S, Katz AE. Salvage cryosurgery of the prostate for failure after primary radiotherapy or cryosurgery: long-term clinical, functional, and oncologic outcomes in a large cohort at a tertiary referral centre. *Eur Urol*. 2013; 64(1):1-7.
10. Lian H, Zhuang J, Yang R, et al. Focal cryoablation for unilateral low-intermediate-risk prostate cancer: 63-month mean follow-up results of 41 patients. *Int Urol Nephrol*. 2016;48(1): 85-90.
11. Cheetham P, Truesdale M, Chaudhury S, Wenske S, Hruby GW, Katz A. Long-term cancer-specific and overall survival for men followed more than 10 years after primary and salvage cryoablation of the prostate. *J Endourol*. 2010;24(7):1123-1129.
12. Gage AA, Baust JG. Cryosurgery for tumors—a clinical overview. *Technol Cancer Res Treat*. 2004;3(2):187-199.
13. Gage AA, Baust JG. Cryosurgery for tumors. *J Am Coll Surg*. 2007;205(2):342-356.
14. Gage AA, Baust J. Mechanisms of tissue injury in cryosurgery. *Cryobiology*. 1998;37(3):171-186.
15. Smith DJ, Fahssi WM, Swanlund DJ, Bischof JC. A parametric study of freezing injury in AT-1 rat prostate tumor cells. *Cryobiology*. 1999;39(1):13-28.
16. Baust JG, Gage AA, Bjerklund Johansen TE, Baust JM. Mechanisms of cryoablation: clinical consequences on malignant tumors. *Cryobiology*. 2014;68(1):1-11.
17. Han B, Bischof JC. Direct cell injury associated with eutectic crystallization during freezing. *Cryobiology*. 2004;48(1):8-21.
18. Sabel MS. Cryo-immunology: a review of the literature and proposed mechanisms for stimulatory versus suppressive immune responses. *Cryobiology*. 2009;58(1):1-11.
19. Hoffmann NE, Bischof JC. The cryobiology of cryosurgical injury. *Urology*. 2002;60(2 suppl 1):40-49.
20. Caso JR, Tsivian M, Mouraviev V, Kimura M, Polascik TJ. Complications and postoperative events after cryosurgery for prostate cancer. *BJU Int*. 2012;109(6):840-845.
21. Baust JG, Gage AA. The molecular basis of cryosurgery. *BJU Int*. 2005;95(9):1187-1191.
22. Baust JG, Gage AA, Klossner D, et al. Issues critical to the successful application of cryosurgical ablation of the prostate. *Technol Cancer Res Treat*. 2007;6(2):97-109.
23. Baust JG, Gage AA, Robilottto AT, Baust JM. The pathophysiology of thermoablation: optimizing cryoablation. *Curr Opin Urol*. 2009;19(2):127-132.
24. Baust JG, Gage AA. Progress toward optimization of cryosurgery. *Technol Cancer Res Treat*. 2004;3(2):95-101.
25. Clarke DM, Robilotto AT, VanBuskirk RG, Baust JG, Gage AA, Baust JM. Targeted induction of apoptosis via TRAIL and cryoablation: a novel strategy for the treatment of prostate cancer. *Prostate Cancer Prostatic Dis*. 2007;10(2):175-184.
26. Clarke DM, Robilotto AT, Rhee E, et al. Cryoablation of renal cancer: variables involved in freezing-induced cell death. *Technol Cancer Res Treat*. 2007;6(2):69-79.
27. Clarke DM, Baust JM, Van Buskirk RG, Baust JG. Addition of anticancer agents enhances freezing-induced prostate cancer cell death: implications of mitochondrial involvement. *Cryobiology*. 2004;49(1):45-61.

28. Hollister WR, Mathew AJ, Baust JG, et al. The effects of freezing on cell viability and mechanisms of cell death in an in vitro human prostate cancer cell line. *Mol Urol*. 1998;2(1):13-18.
29. Han B, Iftekhar A, Bischof JC. Improved cryosurgery by use of thermophysical and inflammatory adjuvants. *Technol Cancer Res Treat*. 2004;3(2):103-111.
30. Han B, Swanlund DJ, Bischof JC. Cryoinjury of MCF-7 human breast cancer cells and inhibition of post-thaw recovery using TNF-alpha. *Technol Cancer Res Treat*. 2007;6(6):625-634.
31. Baust JM, Klossner D, Gage A, VanBuskirk RV, Baust JG. AKT signaling mediates prostate cancer response to cryoablation. *Cryobiology*. 2013;67(3):427-428.
32. Robilotto AT, Baust JM, Van Buskirk RG, Gage AA, Baust JG. Temperature-dependent activation of differential apoptotic pathways during cryoablation in a human prostate cancer model. *Prostate Cancer Prostatic Dis*. 2013;16(1):41-49.
33. Onik G, Porterfield B, Rubinsky B, Cohen J. Percutaneous transperineal prostate cryosurgery using transrectal ultrasound guidance: animal model. *Urology*. 1991;37(3):277-281.
34. Baust JG, Gage AA, Clarke D, Baust JM, Van Buskirk R. Cryosurgery—a putative approach to molecular-based optimization. *Cryobiology*. 2004;48(2):190-204.
35. Thompson I, Thrasher JB, Aus G, et al. Guideline for the management of clinically localized prostate cancer: 2007 update. *J Urol*. 2007;177(6):2106-2131.
36. Aron M, Kamoi K, Remer E, Berger A, Desai M, Gill I. Laparoscopic renal cryoablation: 8-year, single surgeon outcomes. *J Urol*. 2010;183(3):889-895.
37. Jones JS, Rewcastle JC, Donnelly BJ, Lugnani FM, Pisters LL, Katz AE. Whole gland primary prostate cryoablation: initial results from the cryo on-line data registry. *J Urol*. 2008;180(2): 554-558.
38. Baust JG, Bischof JC, Jiang-Hughes S, et al. Re-purposing cryoablation: a combinatorial 'therapy' for the destruction of tissue. *Prostate Cancer Prostatic Dis*. 2015;18(2):87-95.
39. Klossner DP, Robilotto AT, Clarke DM, et al. Cryosurgical technique: assessment of the fundamental variables using human prostate cancer model systems. *Cryobiology*. 2007; 55(3):189-199.
40. Klossner DP, Baust JM, VanBuskirk RG, Gage AA, Baust JG. Cryoablative response of prostate cancer cells is influenced by androgen receptor expression. *BJU Int*. 2008;101(10):1310-1316.
41. Baust JM, Snyder KK, Santucci KL, et al. *Assessment of SCN and argon cryoablation devices in an in vivo like 3-D tissue engineered prostate and renal cancer model. Poster session presented at:. in ACCryo 2014—Advances in Thermal Abaltive Therapy and Biopreservation, Annual Meeting of the American College of Cryosurgery*. FL: Key Largo, 2014.
42. Baust JG, Klossner DP, Vanbuskirk RG, et al. Integrin involvement in freeze resistance of androgen-insensitive prostate cancer. *Prostate Cancer Prostatic Dis*. 2010;13(2):151-161.
43. Gage AA, Baust JM, Baust JG. Experimental cryosurgery investigations in vivo. *Cryobiology*. 2009;59(3):229-243.
44. Robilotto AT, Clarke D, Baust JM, Van Buskirk RG, Gage AA, Baust JG. Development of a tissue engineered human prostate tumor equivalent for use in the evaluation of cryoablative techniques. *Technol Cancer Res Treat*. 2007;6(2):81-89.
45. Robilitto AT, Baust JM, Van Buskirk RG, Gage AA, Baust JG. Differential cell signaling in human prostate cancer cells frozen in monolayers versus a three dimensional prostate tumor model: The PI3 kinase-AKT pathway. *Cryobiology*. 2010; 61(3):364.
46. Hajar R. Animal testing and medicine. *Heart Views*. 2011; 12(1):42.
47. Arora T, Mehta AK, Joshi V, et al. Substitute of animals in drug research: an approach towards fulfillment of 4R's. *Indian J Pharm Sci*. 2011;73(1):1-6.
48. Baust JG, Santucci KL, Snyder KK, et al. Tissue Engineered Model and Method of Use, USPTO patent 9,213,025. Issued December 15, 2015, CPSI Holdings LLC.
49. Healthtronics, V. Probe: 5 position variable cryoprobe, in 2011; https://www.healthtronics.com/sites/default/files/resources/V-probe-Instrument-Sheet.pdf. Updated August 2011, Accessed April 2017. Austin, TX.